Science of the Total Environment 724 (2020) 138191

Contents lists available at ScienceDirect

Science of the Total Environment

journal homepage: www.elsevier.com/locate/scitotenv

Zinc isotope revealing zinc's sources and transport processes in karst region

Yafei Xia [a,b,1], Ting Gao [a,b,1], Yuhui Liu [a,b], Zhengrong Wang [d], Chengshuai Liu [a,c,e,f,*], Qiqi Wu [c,e,f], Meng Qi [a,b], Yiwen Lv [c,e,f], Fangbai Li [c,e,f]

[a] State Key Laboratory of Environmental Geochemistry, Institute of Geochemistry, Chinese Academy of Sciences, Guiyang 550081, PR China
[b] University of Chinese Academy of Sciences, Beijing 100049, PR China
[c] Guangdong Key Laboratory of Integrated Agro-Environmental Pollution Control and Management, Guangdong Institute of Eco-Environmental Sciences & Technology, Guangzhou 510650, PR China
[d] Department of Earth & Atmospheric Sciences, City College of New York, CUNY, New York 10031, USA
[e] National-Regional Joint Engineering Research Center for Soil Pollution Control and Remediation in South China, Guangzhou 510650, PR China
[f] Guangdong Academy of Sciences, Guangzhou 510650, PR China

HIGHLIGHTS

- Tailings, rivers, sediments, dusts and soils were analyzed for Zn isotope ratios.
- Anthropogenic Zn in karst area was mainly from dust through physical transmission.
- Zn in paddy soil was imported by long-term wind dispersion of fine-grained material.
- Pollution sources and pathways of heavy metals can be traced using Zn isotopes in karst area.

GRAPHICAL ABSTRACT

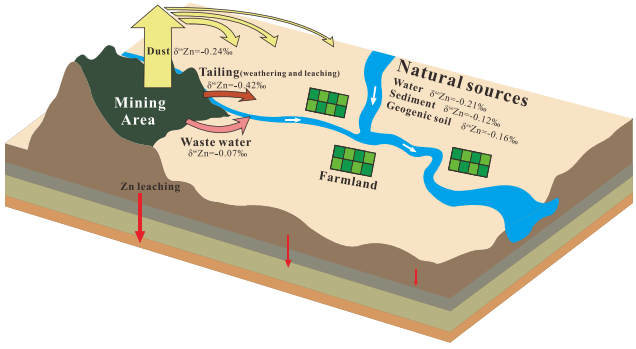

ARTICLE INFO

Article history:
Received 30 January 2020
Received in revised form 23 March 2020
Accepted 23 March 2020
Available online 25 March 2020

Warning: Editor name is missing. Please check.

Keywords:
Zinc isotope
Karst area
Mining
Heavy metals

ABSTRACT

The heavy metal pollution, mainly caused by mining-related activities over extended period of time, is imposing a severe threat to environments and human health. Environmental systems, including rivers and paddy soils, have been widely established as one of the key sinks of potentially harmful metals. Aiming to understand contamination sources and pathways of Zn in karst area, we studied the Zn concentration and isotope composition of river waters, sediments, mine tailings, paddy soils, dust and three soil profiles with different levels of Zn-pollution around a Zn-mine, southwestern China. The distinct Zn isotope compositions among tailing (-0.42 ± 0.02‰), dust (-0.24 ± 0.02‰), and geogenic soil (-0.16 ± 0.03‰) allowed for separation of anthropogenic-Zn from native Zn. In the plot of δ^{66}Zn value and 1/Zn, all samples can be explained by the mixing of three components: mining-input, agricultural input, and background. Evolution of these three components helps produce direct sources: dust and geogenic soil. Under this framework, the Zn pollution in paddy soil and sediment can be explained by mixing of mine-tailing, dust, and geogenic soil. Our study shows that the contamination of mine drainage is limited in the area due to the relatively high pH buffered by carbonate in karst area. While the dust contributes most of the anthropogenic Zn with an average value of 19.5%. The dominant pathway of

* Corresponding author at: State Key Laboratory of Environmental Geochemistry, Institute of Geochemistry, Chinese Academy of Sciences, Guiyang 550081, PR China.
E-mail address: liuchengshuai@vip.gyig.ac.cn (C. Liu).
[1] Yafei Xia and Ting Gao contributed equally to this work.

https://doi.org/10.1016/j.scitotenv.2020.138191

Dust
Paddy soil

anthropogenic Zn from dust to paddy soil or sediment is through the long-term wind dispersion of fine-grained material from the tailing and the physical transmission. Under the special hydrogeological conditions of karst, mining activities will increase the migration of heavy metals. The Fe-Al oxides control the migration of Zn in soil profile, but probably do not lead to significantly Zn isotopes fractionation. This further enhances the reliability of Zn isotopes as a "fingerprint" in karst area.

1. Introduction

Large-scale mineral resources occur near or in karst landforms in southwestern China. Despite their great economic values, the industrial-scale mineral excavation and refining have imposed serious environmental issues — heavy metal pollution — to ambient environments and environments downstream of Chinese major rivers (e.g. Pearl river) (e.g. Li et al., 2014). Long-term mining and metallurgical operations have generated large amounts of wastes and derivatives including mine tailing, acid mine drainage, and dust (Qin et al., 2012; Pu et al., 2019), from which heavy metal ions are readily dissolved under an oxidized atmosphere, resulting into contamination in water and soil.

In addition to human activities, soils on karst area are especially vulnerable to degradation and heavy metal pollution due to their low environmental capacity, poor stability, and low disaster-bearing capacity (Wang et al., 2004). Most carbonate rocks in karst region of southwest China were formed before the Mesozoic. They are nutrient-poor and easily eroded (Moore et al., 2017). Karst formation in southwestern China is a well-known area containing anomaly high concentration of heavy metals (Ruan et al., 2013). Under the subtropical climate conditions with intensive precipitation from Indian monsoon every year in southwestern China, heavy metal ions are spreading widely due to the high permeability of carbonate rocks (e.g., Peng and Wang, 2012; Chen et al., 2015). The ill-advised social and economic activities of human beings further intensify the threats to the environment and human health (Zhang et al., 2016). Thus, a better understanding of the source and transport process of the heavy metal pollution could help develop policies to reduce the threats of heavy metal pollution in karst area.

The sources and transport processes of heavy metals have received long-term attentions for their environmental concerns (Marrugo-Negrete et al., 2017). At present, three common research methods include the statistical method (e.g. Yun et al., 2016; Li et al., 2017), geochemical mapping method (e.g. Khalil et al., 2014; Guagliardi et al., 2015), and isotope tracer method (e.g. Juillot et al., 2011; Viers et al., 2015; Aucour et al., 2017), are widely used for examining pollution sources. The first two methods, as traditional tracing methods, are mainly to analyze/evaluate the total amount of heavy metals and their chemical forms in soil (Sun et al., 2018). Although these traditional data-processing methods based on concentrations can help identify the source of pollution in soil, such analyses require a large dataset and can hardly yield reliable quantitative results (Pu et al., 2017). These restrictions of the traditional methods, as well as the complex conditions in natural systems, may become the main challenges in identifying the sources of heavy metals and their migration processes. While the isotopic technique, with high accuracy and resolution, has an advantage in tracing multi-source pollution in complex wild environments (Moynier et al., 2017).

With the continuous improvement of isotope analysis techniques and equipment, many stable metal isotopes have been developed to trace geological and environmental processes (e.g. Wiederhold, 2015). Among them, zinc (Zn) isotope systematics has received particular interests in the past two decades due to the significant Zn isotope fractionation in many biogeochemical processes, such as core formation (Bridgestock et al., 2014), mantle melting (Wang et al., 2017), chemical weathering (Lv et al., 2016), ocean nutrient circulation (Vance et al., 2019; Sieber et al., 2020), paleo-environment reconstruction (Pons et al., 2011, 2013), and plant physiological processes (Arnold et al., 2015; Wiggenhauser et al., 2018). In particular, Zn isotopes are widely used to fingerprint the sources and routes of heavy metal contamination in recent years (Moynier et al., 2017; Li et al., 2019). For example, Araújo et al. (2017) used Zn stable isotope composition to identify anthropogenic Zn sources in coastal environments. They found that spatial and temporal analysis of sediment samples fit well in a model of mixing involving three main end-members. Bigalke et al. (2013) demonstrated that Zn isotopes can be used to trace the mobilization and sources of Zn in intertidal soils. They suggested that excavation might be the major source of Zn pollution, with a small or no contribution from smelters or smelter wastes. Similarly, Fekiacova et al. (2015) traced the contamination sources in soils using Zn isotopes and found that Zn isotope ratios in surface soils are characterized mostly by anthropogenic signatures, while the deep soils are similar to the local background value.

This study focuses on the Niujiaotang mine in Duyun County, Guizhou Province, southwestern China. It is a Pb-Zn deposit exposed in the typical karst region of China. The mining activities produced significant heavy metal pollution to the local environments, and source of the pollution has great uncertainty. To solve these problems, we systematically investigate the Zn isotope compositions of river waters, sediments, soils, dust, mine tailings, ores, and bedrocks. Our main objectives are to understand 1) how Zn was transported from mining area to surrounding environments; and 2) how Zn behaves after being discharged into soils. Our findings would help improving our knowledge about the behavior of Zn during the migration into paddy soils which provides scientific implications and bases for how to remediate soil pollution by heavy metals in karst area.

2. Site description and sample collection

This study was carried out around the Zn mine of Niujiaotang in Duyun County, Guizhou Province in southwestern China (107°30′59″ E, 26°15′46″N; Fig. 1). This region is characterized by subtropical, humid, and monsoonal climate, with a mean annual temperature of ~16.4 °C and mean annual precipitation of ~1418.7 mm (averaged between 1981 and 2010; all data were collected from China Meteorological Administration, http://data.cma.cn/). Carbonate rocks are widely distributed in this area and were karstified over geological timespans, forming a typical karst landform. The main ore minerals in this area include sphalerite, smithsonite, pyrite, and galena, the wall surrounding rock is mainly composed of dolomite (Ye, 2001; Zhang et al., 2018). Since the 20th century, large scale mining for Zn ores has taken place in the area, resulting in a great threat to the health of local people.

A total of eight sampling sites were chosen along two rivers: 1) Fanjia river (sites #1 through #5, from the core mining area to the downstream); 2) Caiyuan river (site #6) which was not appreciably affected by mining activity (Fig. 1 and Table 1); 3) Sites #7 and #8 were selected after two rivers merges near Xiaozhaizi. River water, sediment, and paddy soil samples were collected at these sites. Sediments were sampled at river bed and paddy soils were sampled from topsoil. Prior to sampling, water sample bottles were washed with ~3% HNO_3 (m/m) and rinsed with pure water three times. Tailings, Zn-ores, and wastewater were collected in mining area. Dust was collected on pre-cleaned

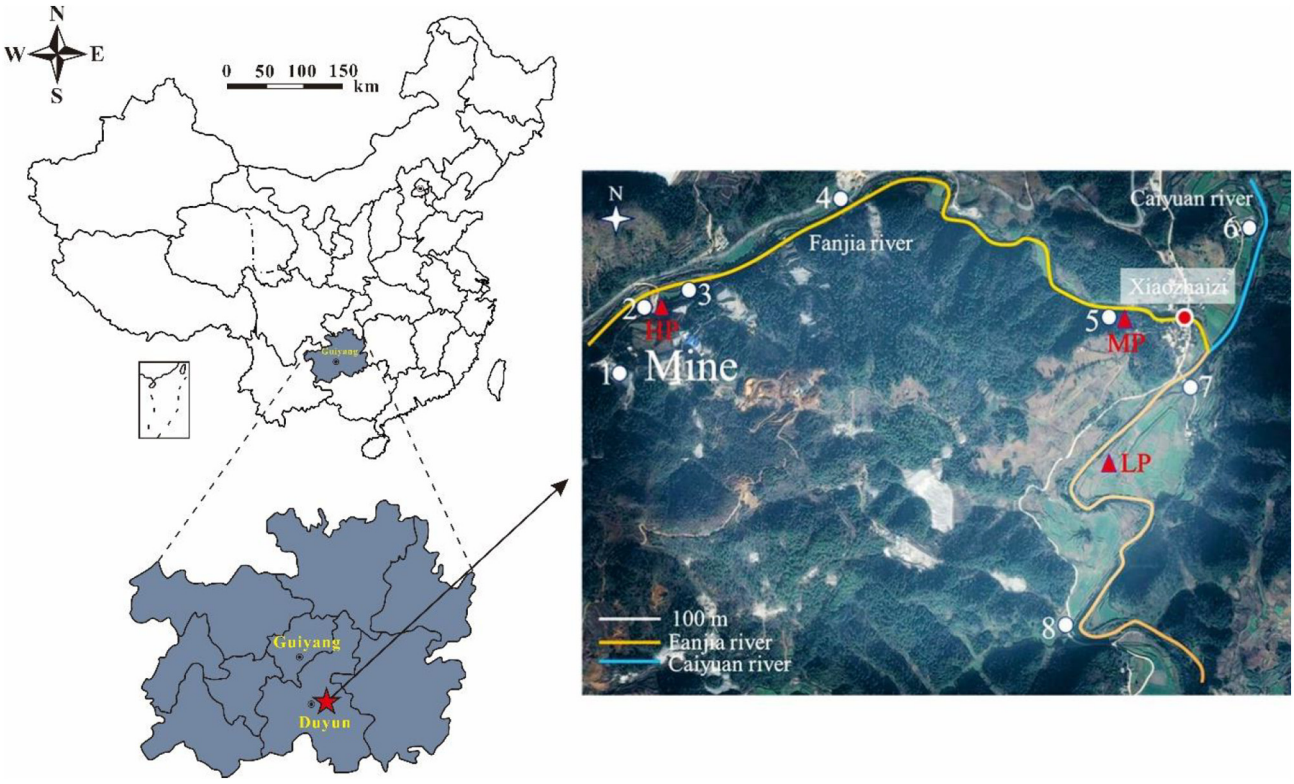

Fig. 1. Map of the study area and location of the study sites in Guizhou Province, China. The white circles represent the sampling sites (#1 to #8) along the Fanjia and Caiyuan rivers. The red triangles represent the sampling sites of paddy soil profiles. (For interpretation of the references to color in this figure legend, the reader is referred to the web version of this article.)

Whatman® 41 cellulose filter (Φ = 50 mm) by AKFC-92A sampler (Changshu Mine Mechanical and Electrical Equipment Co. LTD). Then the filters with samples were sealed in airtight plastic bags (Franssens et al., 2004). Geogenic soils and bedrocks were collected in places without any appreciable mining interferences and pollutions. Fertilizer samples used for rice were also collected. After sampling, samples were immediately sealed in airtight plastic bags, and transported to the laboratory within 24 h. In the lab, diluted distilled nitric acid was added to water samples to adjust pH < 2, then filtered and put into 4 °C refrigerator. All solid samples were air-dried and ground to pass through a nylon sieve of 200 mesh.

Three soil profiles with different levels of contamination were also sampled along the river (with named HP, MP, and LP refer to high, medium, and low levels of contamination, respectively. Fig. 1). According to the depth of profile as well as the color and texture of soils, seven, six and eight samples were collected in HP, MP, and LP profile, respectively.

Table 1
Key physicochemical properties of samples.

Sample site	Paddy soil			Sediment			Water	
	pH	Eh (mV)	TOC (g/kg)	pH	Eh (mV)	TOC (g/kg)	pH	Eh (mV)
1	5.99	63.9	4.73	-	-	-	-	-
2	6.72	26.3	23.51	6.03	51.9	26.31	8.77	−95.6
3	-	-	-	6.26	49.3	31.00	8.74	−96.5
4	6.69	28.0	18.10	6.35	46.1	52.31	8.87	−101.6
5	6.88	17.2	34.76	6.92	12.8	28.78	8.95	−106.0
6	6.51	38.5	24.04	6.67	27.1	7.44	8.62	−87.5
7	5.48	97.1	20.32	6.76	20.5	16.03	8.71	−92.6
8	6.64	30.8	18.69	6.94	12.6	7.84	8.65	−89.2

Sample type	pH	Eh (mV)
Geogenic soil, bed-rock, fertilizer		
Geogenic soil	6.93	14.3
Geogenic soil	6.93	14.2
Geogenic soil	6.94	13.5
Geogenic soil	6.85	19.2
Bed-rock	-	-
Bed-rock	-	-
Fertilizer	5.10	125.9
Mine materials		
Tailing	-	-
Tailing	-	-
Zn-ore	-	-
Mine drainage	8.02	−55.0
Dust	-	-
Dust	-	-

-: no measurement or inexistence.

3. Materials and methods

3.1. Eh, pH and TOC analysis

The pH and Eh values of soils and sediments were measured by putting ~10 g of solid powders in ~25 mL of Millipore water (~18.2 MΩ). Total organic carbon (TOC) content was determined by an elemental analyzer (vario MACRO cube, Elementar, Germany). Prior to analysis, samples were treated with ~3% HCl (v/v) to remove inorganic carbon.

3.2. Sample digestion

About 20 mg of powder samples (>200 mesh) were first weighted in Savillex® Teflon breakers and then digested by using a combination of distilled HF-HNO_3-HCl, using a procedure modified after Gao et al. (2018). Each sample was first treated with a 3:1 (v/v) of HF-HNO_3 and heated at ~180 °C for ~16 h. After samples were cooled to room temperature, they were evaporated to dryness at ~160 °C. Samples were then dissolved in a mixture of HCl and HNO_3 (3:1, v/v), followed by heating at ~140 °C for a complete digestion and evaporated to dryness at ~80 °C subsequently. The cellulose filter with dust particles was

mineralized by HNO_3-HF-HCl (4:1:1 v/v) on a hot plate based on the method of Franssens et al. (2004). Then, 1–2 mL of 30% H_2O_2 was added and covered on a hot plate at 70 °C for 1 h to completely digested before being evaporated to dryness at ~80 °C. Finally, each sample solution was split into two aliquots, which were dissolved in ~3% HNO_3 (m/m) for Zn concentration analysis and ~8 N HCl for column purification, respectively. About 20–100 mL water samples were evaporated/concentrated in Savillex® beakers based on the method from Borrok et al. (2007). The evaporated samples were then dissolved in a mixture of HCl and HNO_3 (3:1, v/v), followed by heating at ~140 °C and then evaporated to dryness at ~80 °C subsequently. Finally, samples were dissolved in ~8 N HCl for column purification.

3.3. Sequential extraction experiment

The Zn speciation in paddy soils and sediments were analyzed using five-step sequential extraction method following Tessier et al. (1979). About 1 g of solid sample was weighted in a 50-mL centrifuge tube before the reagents were added sequentially. The detailed procedures are shown in Table 2. After each extraction step, the tube was centrifuged at 9168 ×*g* for ~30 min (Sigma 3K15, Germany) and then the supernatant in the tube was extracted by a transfer pipette. The solutions (F1, F2, F3, and F4) were first transferred into Savillex® breakers to dry down before they were dissolved in ~1 mL 16 N HNO_3 for converting to nitrate salts. Afterwards, the samples were dried again and re-dissolved in ~3% HNO_3 (m/m) for elemental analysis. The residues after extraction were washed three times with deionized water and dried with a freeze dryer (Alpha 1–4 LDplus, Germany) before being grounded into fine powders, 20 mg of which (F5) were weighted in the Savillex® breakers and digested using the same procedures as described in Section 3.2.

3.4. Element concentration analysis

Element concentration analysis was conducted at the Guangdong Institute of Eco-environmental Science & Technology, Guangzhou, China. Major elements (including Al, Ca, Fe, and Mg) concentration were determined by the inductively coupled plasma optical emission spectroscopy (ICP-OES, PerkinElmer® Optima 8000, USA). Trace elements (including Cd, Cr, Cu, Pb, and Zn) were determined by the inductively coupled plasma mass spectrometry (ICP-MS, PerkinElmer® NexION 300X, USA). Reference materials (BHVO-2 and AGV-2) were used as external standards for quality control of measured major elements. The measured concentrations of the trace elements were corrected with the addition of Sc as an internal standard. Multi-element standard solutions were used to establish calibration curves.

3.5. Zinc purification and isotope analysis

Pure Zn solutions were separated by chromatographic columns in a class-1000 clean room equipped with class-100 laminar flow hoods in the Guangdong Institute of Eco-environmental Science & Technology, Guangzhou, China. The purification procedure has been reported in Lv et al. (2016). Briefly, samples containing about 1–5 μg of Zn were loaded onto the column stuffed with ~2 mL AG MP-1 resin (100–200 mesh, Bio-Rad, USA). The resin was pre-cleaned by ~8 N HCl, ~0.5 N HNO_3, and Milli-Q water, alternatively. Matrix elements were removed by washing first with ~8 N HCl and then with ~2 N HCl. Zn was collected in the following ~10 mL of ~0.5 N HNO_3 after ~2 mL of ~0.5 N HNO_3. The same column procedure was repeated twice to obtain a pure Zn solution for isotopic analyses. The geological reference materials BHVO-2 and AGV-2 were processed together with samples for each batch of column chemistry. The total procedural blanks (from sample dissolution to mass spectrometry) were routinely measured and had a long-term average of ~10 ng (n = 12) for Zn, which is considered neglected during mass spectrometry. Zn separates were dries at ~80 °C followed by the addition of ~1 mL 16 N HNO_3 to remove HCl, and finally re-dissolved in ~1 mL ~3% HNO_3 (m/m) for isotopic analysis.

Zn isotope analysis was carried out on a Neptune Plus MC-ICP-MS (Thermo Scientific, USA) at the Institute of Geochemistry, Chinese Academy of Sciences, China, using a wet plasma and the sample-standard bracketing (SSB) method (e.g. Marechal et al., 1999; Liu et al., 2016). Zn isotope ratios were measured in the low-resolution mode with a high sensitivity (X) nickel cone. The 1-ppm solution typically yielded a beam intensity of ~15 V for ^{64}Zn. Prior to analysis, both samples and standards were adjusted to ~200 ppb in ~3% HNO_3 (m/m). Isotopic ratios were obtained for 1 block of 90 cycles with ^{64}Zn in the L2 cup, ^{66}Zn in the central cup, ^{67}Zn in the H1 cup, and ^{68}Zn in the H2 cup. Each sample was measured three times to achieve a better reproducibility. All Zn isotope compositions of samples in this work were expressed as the differences in $^{66}Zn/^{64}Zn$ between sample and standard IRMM-3702 through $\delta^{66}Zn = [(^{66}Zn/^{64}Zn)_{sample} / (^{66}Zn/^{64}Zn)_{IRMM\text{-}3702} - 1] \times 1000$. The geological reference materials BHVO-2 and AGV-2 yielded average $\delta^{66}Zn$ values of 0.054 ± 0.07‰ and 0.064 ± 0.016‰, respectively, which were consistent within uncertainty with previously published results (e.g. Balistrieri et al., 2008; Bigalke et al., 2010; Lv et al., 2016; Wang et al., 2017).

4. Results

4.1. Sample properties

The physicochemical properties of soils, sediments, mine tailings and river waters are listed in Table 1. The pH values of river waters range from 8.62 to 8.95, significantly higher than mine drainage (~8.02). The sediments have pH values ranging from 6.03 to 6.94, showing an increasing trend from the core mining area to the downstream (from site #1 through #5 in Table 1). The pH values of paddy soils vary from 5.48 to 6.88. By contrast, the geogenic soils display a relatively narrow pH range, varying from 6.85 to 6.94.

The TOC values of sediments in Fanjia river system change from 26.31 to 52.31 g/kg, higher than the relatively unpolluted Caiyuan river (7.44–16.03 g/kg). The TOC values of paddy soils range from 4.73 to 34.76 g/kg with an average value of 20.59 g/kg.

The pH, Eh, and TOC of soil samples in three profiles are displayed in Table 3. The pH values of soil samples in HP, MP, and LP profiles display a relatively narrow range from 6.61 to 6.94, 6.71 to 7.45, and 5.13 to 7.39, respectively. The TOC values of these samples in three profiles show an increasing trend towards the surface horizon, ranging from 7.78 to 20.51 g/kg, 3.85 to 38.78 g/kg, and 3.40 to 21.53 g/kg, respectively.

Table 2
Sequential extraction procedures of Tessier.

	Fractions	Reagents	Conditions
F1	Exchangeable fraction	1 M $MgCl_2$, pH 7.0	20 ± 1 °C, 1 h shaking
F2	Carbonate fraction	1 M NaAc, pH 5 (HOAc adjust)	20 ± 1 °C, 6 h shaking
F3	Iron & manganese oxides fraction	0.04 M $NH_2OH{\cdot}HCl$ in 25% (v/v) HOAc, pH 2.0	96 ± 3 °C, 6 h shaking
F4	Organic matter fraction	0.02 M HNO_3 + 30% H_2O_2, pH 2.0	85 ± 2 °C, 5 h shaking
F5	Residual	HF-HCl-HNO_3	Digestion

Table 3
Key physicochemical properties, metal concentration, and Zn isotope composition of soils samples in three profiles.

Sample name	Depth (cm)	pH	Eh (mV)	TOC	Al	Ca	Fe	Mg	Zn	δ^{66}Zn (‰)	2SD	N[a]
				(g/kg)								
Highly polluted area												
HP-0	60–90	6.82	20.7	10.99	62.73	28.85	56.66	17.92	2.53	−0.14	0.04	3
HP-1	50–60	6.93	14.3	15.01	79.93	16.05	61.27	12.63	3.34	−0.37	0.04	3
HP-2	40–50	6.93	14.2	7.78	93.04	7.52	76.97	8.49	3.93	−0.37	0.02	3
HP-3	30–40	6.94	13.5	16.47	61.42	29.73	55.05	20.51	3.29	−0.25	0.01	3
HP-4	20–30	6.85	19.2	12.52	69.36	28.14	60.48	18.93	3.47	−0.33	0.04	3
HP-5	10–20	6.64	31	20.51	53.31	49.76	53.40	30.70	4.44	−0.31	0.02	3
HP-T[b]	0–10	6.61	33.2	19.49	52.25	49.60	50.80	30.84	4.68	−0.29	0.04	3
Moderately polluted area												
MP-0	50–80	7.34	−11.3	3.85	34.10	131.87	45.55	47.70	1.63	−0.24	0.07	3
MP-1	40–50	7.45	−17	13.39	50.20	79.41	62.14	29.82	2.27	−0.22	0.02	3
MP-2	30–40	7.41	−14.7	21.37	58.50	43.62	75.69	257.15	2.99	−0.31	0.01	3
MP-3	20–30	6.83	19.8	31.16	51.66	55.53	70.75	33.02	3.16	−0.27	0.03	3
MP-4	10–20	6.77	24.5	33.85	50.52	585.56	70.72	34.34	3.08	−0.30	0.01	3
MP-T[b]	0–10	6.71	26.8	38.78	47.46	45.14	63.39	27.69	2.84	−0.27	0.02	3
Least polluted area												
LP-0	80–100	7.39	−12.1	3.4	64.59	2.23	41.92	7.69	0.26	−0.13	0.03	3
LP-1	70–80	7.32	−8.1	5.26	61.04	2.45	40.25	7.07	0.30	−0.14	0.03	3
LP-2	60–70	6.94	13.5	5.93	61.41	2.48	40.04	7.02	0.28	−0.17	0.03	3
LP-3	50–60	7.25	−4.1	6.52	60.81	2.56	38.26	6.92	0.22	−0.15	0.02	3
LP-4	40–50	7.24	−3.9	6.6	51.03	3.57	35.13	6.07	0.18	−0.17	0.03	3
LP-5	30–40	7.1	1.3	3.99	62.18	2.22	48.13	6.93	0.26	−0.11	0.01	3
LP-6	20–30	7.16	0.8	11.05	61.33	3.32	50.36	6.83	0.42	−0.08	0.01	3
LP-T[b]	0–20	5.13	117.1	21.53	67.04	15.09	51.03	7.33	0.54	−0.12	0.05	3

[a] N refers to the times of repeat measurements of the same purification solutions by MC-ICP-MS.
[b] T refers to the topsoil of each profile.

Table 4
Metal concentration and Zn isotope composition of samples.

Sample name	Sample type	Al	Ca	Fe	Mg	Zn	δ^{66}Zn (‰)	2SD	N[a]
		(g/kg)							
R-1	Paddy soil	1.51	175.73	60.83	102.33	6.93	−0.33	0.02	3
R-2	Paddy soil	51.06	53.69	49.84	32.52	4.40	−0.28	0.02	3
R-4	Paddy soil	54.76	56.50	53.14	35.46	4.69	−0.26	0.01	3
R-5	Paddy soil	31.83	76.85	53.56	46.74	2.17	−0.29	0.03	3
R-6	Paddy soil	59.76	64.38	85.58	39.32	3.78	−0.29	0.02	3
R-7	Paddy soil	65.62	6.25	58.20	6.46	2.36	−0.20	0.02	3
R-8	Paddy soil	49.70	2.42	24.56	5.17	0.34	−0.29	0.02	3
S-2	Sediment	11.77	188.17	28.32	106.63	10.22	−0.22	0.02	3
S-3	Sediment	21.43	139.25	33.65	55.17	1.66	−0.36	0.02	3
S-4	Sediment	29.22	108.97	35.91	50.03	4.21	−0.28	0.03	3
S-5	Sediment	28.97	123.85	43.47	53.94	2.64	−0.32	0.02	3
S-6	Sediment	44.60	50.47	30.00	26.24	0.76	−0.12	0.03	3
S-7	Sediment	40.01	86.16	33.00	36.77	1.61	−0.25	0.00	3
S-8	Sediment	53.02	39.41	32.91	18.85	0.54	−0.26	0.01	3
GS 1	Geogenic soil	61.04	2.45	40.25	7.07	0.30	−0.14	0.03	3
GS 2	Geogenic soil	61.41	2.48	40.04	7.02	0.28	−0.17	0.03	3
GS 3	Geogenic soil	60.81	2.56	38.26	6.92	0.22	−0.15	0.02	3
GS 4	Geogenic soil	51.03	3.57	35.13	6.07	0.18	−0.17	0.03	3
Dust1	Dust	ND	29.73	11.81	21.21	13.40	−0.22	0.05	3
Dust2	Dust	ND	43.62	18.43	24.80	11.73	−0.26	0.00	3
Zn-ore	Zn-ore	ND	61.42	4.39	54.21	61.34	−0.23	0.03	3
Tailing1	Tailing	ND	154.57	17.06	104.26	17.75	−0.39	0.04	3
Tailing2	Tailing	0.01	95.98	56.04	57.69	183.97	−0.44	0.02	3
Fertilizer	Fertilizer	5.43	5.64	1.60	7.71	0.02	0.01	0.05	3
Bed-rock1	Bed-rock	ND	58.31	1.81	61.60	0.06	−0.45	0.02	3
Bed-rock2	Bed-rock	ND	42.25	0.86	32.38	0.17	−0.42	0.07	3
BHVO-2	Reference material	72.00	79.90	85.90	43.30	0.11	0.054	0.07	3
AGV-2	Reference material	78.62	37.11	46.66	12.52	0.08	0.064	0.02	3
W1	Mine drainage	0.1859	167.88	0.0035	99.12	1.706	−0.07	0.03	3
W2	River water	0.1091	65.44	0.0130	35.4	0.1394	−0.08	0.02	3
W3	River water	0.1116	55.36	0.0110	30.58	0.0303	−0.07	0.03	3
W4	River water	0.1185	55.72	0.0130	30.43	0.0295	−0.08	0.02	3
W5	River water	0.1092	59.32	0.0124	32.72	0.0298	−0.13	0.01	3
W6	River water	0.1683	44.53	0.0406	25.25	0.0506	−0.21	0.02	3
W7	River water	0.1662	50.64	0.0498	28.34	0.0304	−0.20	0.00	3
W8	River water	0.1046	37.78	0.0234	20.97	0.0195	−0.19	0.03	3

-: no measurement or inexistence. ND: below the limit of detection.
[a] N refers to the times of repeat measurements of the same purification solutions by MC-ICP-MS.

4.2. Variations of Zn concentrations

The mine waste including dust, ore debris, and mine tailings exhibit significantly high concentrations of Zn with average values of 12.57, 61.34, and 100.59 g/kg, respectively (Table 4). By contrast, geogenic soils and bed-rocks both have relatively lower concentration of Zn, with average values of 2.46 g/kg and 1.14 g/kg, respectively.

Among water samples, Zn concentrations are relatively low and without a significant variation (0.02–0.14 mg/L), except for the mine drainage (W1) which has a comparatively high concentration of Zn (~1.71 mg/L).

In the sediments of Fanjia river system, a high concentration of Zn is accumulated in site #2 (10.22 g/kg) where both wastewater and Fanjia river contribute (Table 4). Along the river, the concentration of Zn decreases from 10.22 to 0.54 g/kg, with an average value of ~3.09 g/kg. The Zn distribution patterns among solutions from the five sequential leaching steps in sites #5 through #8 are similar to each other, while the concentration of Zn extracted during the F2 step decreases successively in the first three sediments (Fig. 2A).

Metal concentrations of paddy soils are summarized in Table 4. The Zn concentrations in bulk paddy soils decrease with the increasing distance from the mining area, ranging from 6.93 to 0.34 g/kg, while the concentration of Zn extracted in F2 decreases but in F5 increases towards the downstream (Fig. 2B).

The metal concentrations of soils from the three profiles are listed in Table 3. The concentration of Zn in all three profiles shows a continuous decrease from the surface to bottom, ranging from 2.53 to 4.68 g/kg, 1.63 to 3.16 g/kg, and 0.18 to 0.54 g/kg, respectively. Zn is most abundant in the residue (step F5) and the concentration of Zn bounded to carbonates (step F2) decreases from the surface towards bottom, and from areas with high to low level of pollution (Fig. 2C).

4.3. Variations of Zn isotope ratios

Zn isotope compositions of all samples except those from the three profiles are presented in Table 4. The average δ^{66}Zn value of the bedrocks is −0.44 ± 0.02‰, which is identical to mine tailings (−0.42 ± 0.02‰). Zn-ores have an average δ^{66}Zn value of −0.23 ± 0.03‰, which is consistent with that of dust (−0.24 ± 0.02‰). The mine drainage (−0.07 ± 0.03‰) is enriched in heavy isotopes relative to other samples of mining wastes. The δ^{66}Zn values of geogenic soils and fertilizer are −0.16 ± 0.03‰ and 0.01 ± 0.05‰, respectively.

The Zn isotope compositions of Fanjia River water samples range from −0.13 to −0.07‰ with an average value of −0.09 ± 0.05‰. Sediments in Fanjia river have variable δ^{66}Zn values from −0.36 to −0.22‰, with an average value of −0.29 ± 0.16‰. In Caiyuan river, waters are characterized by a uniform Zn isotope composition (−0.21 to −0.19‰), which is lighter than that of the Fanjia river waters. The Zn isotope compositions of sediments range from −0.26 to −0.12‰. Sediment of site #6 that was not appreciably affected by mining activity have slightly heavier Zn isotope compositions (−0.12‰) than sites #7 and #8 (−0.26 to −0.25‰).

The δ^{66}Zn values of the top-soils range from −0.33 to −0.20‰ with an average of −0.28 ± 0.08‰. Zn isotope compositions of soil samples from profiles HP, MP, and LP are reported in Table 3. These three profiles have δ^{66}Zn value ranging from −0.37 to −0.25‰, −0.31 to −0.22‰, and − 0.17 to −0.08‰, respectively. In the HP profile, the upper layer of profile has a uniform δ^{66}Zn value (−0.12 to −0.08‰), while the

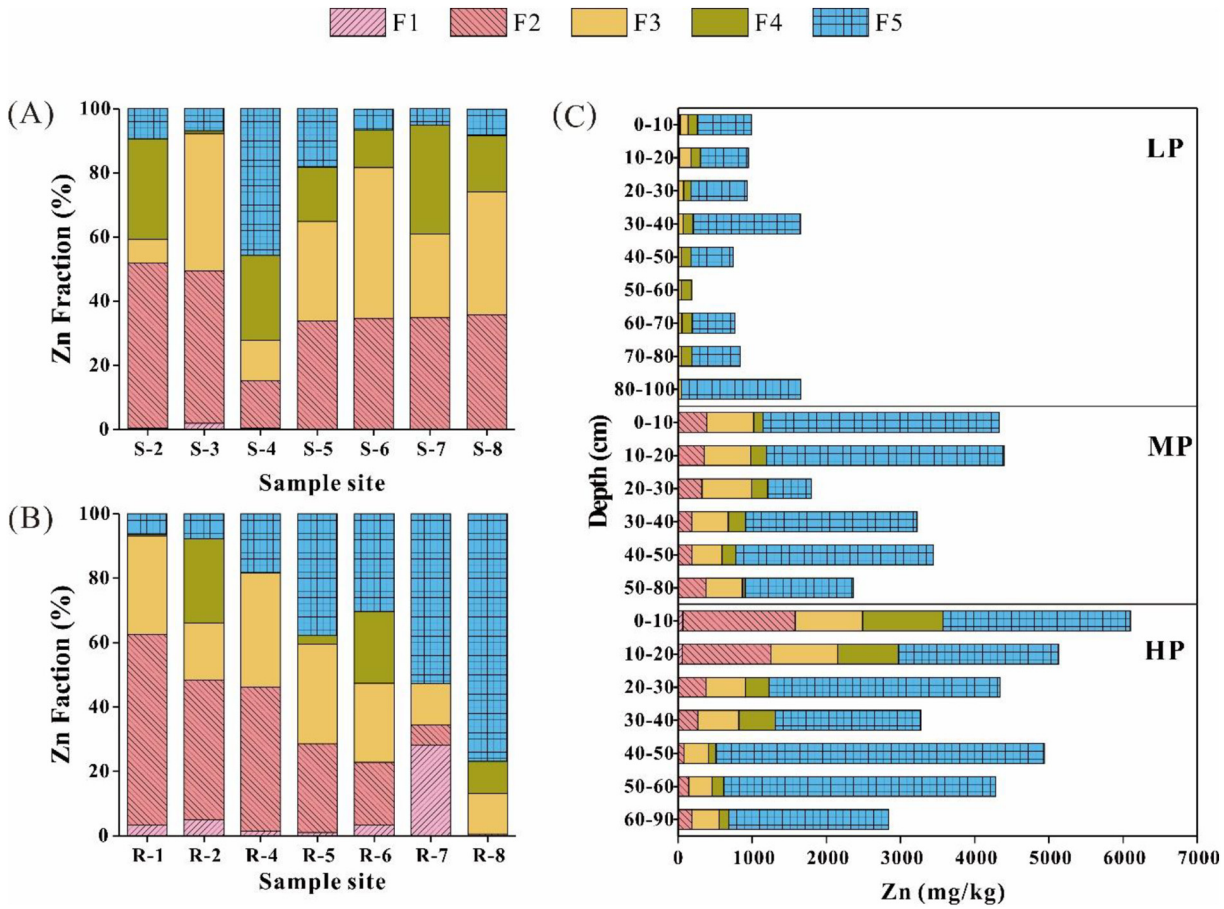

Fig. 2. Distribution of different Zn forms in (A) sediment, (B) paddy soil, and (C) soil profiles. F1: Exchangeable fraction, F2: carbonate fraction, F3: Fe-Mn oxide fraction, F4: organic fraction, and F5: residual fraction.

deepest soil shows isotopically lighter Zn than upper soils but isotopically consistent with geogenic soils (−0.16 ± 0.034‰). In the MP profile, the δ^{66}Zn value changes slightly at the depth of 0–40 cm. It then increases towards to geogenic soil. In the LP profile, the δ^{66}Zn value of soil changes limitedly within uncertainty from the bottom to surface, which is similar to that of geogenic soils.

5. Discussion

5.1. Provenance and transport of Zn

Acid mine drainage (particularly those associated with metal-sulfide ores) represents one of the most important sources of heavy metal contamination to river systems (Simate and Ndlovu, 2014; Dorin and Bunce, 2015; Yang et al., 2019). However, in our study area, the mine drainage (W1) has a pH value of ~8.02, which was resulted from the neutralization by dissolution of carbonate rocks with the wall rock of dolomite (Lewis, 2004). This is consistent with the observation by Stromberg and Banwart (1999) who suggested that the acid drainage produced by sulfide mineral oxidation can be partially or completely offset by carbonate rock in karst area, resulting in neutral or weak alkaline mine water. The mine drainage has a δ^{66}Zn value of −0.07 ± 0.03‰, which is heavier than that of the Zn-ores (−0.23 ± 0.03‰) and tailings (−0.42 ± 0.02‰). This is consistent with the observation that isotopically heavy Zn is preferentially released into the water phase during dissolution of rocks and minerals (Fernandez and Borrok, 2009). In addition, most of Zn in ore is released during the washing process, so the isotope composition of the wastewater should be little different from the minerals.

All river water samples have low Zn content, which may result from the strong adsorption and weak dissolution property of heavy metals under the alkaline condition of river in karst area (Sherene, 2010; Flora et al., 2011). For the Fanjia river, waters have uniform δ^{66}Zn value (−0.13 to −0.07‰) (Fig. 3), which is identical to that of the mine drainage. This indicates that no physicochemical activities are present to fractionate Zn isotopes over a short distance when the mine wastewater is discharged into the Fanjia river. Similar observations were also reported by Balistrieri et al. (2008) and Aranda et al. (2012). It should be noted that the sediments in the polluted Fanjia river are enriched in light Zn isotopes compared to river water. While the sediment in the unpolluted site #6 is enriched in heavy Zn isotopes relative to river water (Fig. 3). The sediments of Fanjia river have high Zn content with Zn isotope signal consistent with dust and Zn-ore, which strongly shows the influence of mining. This anthropogenic Zn input changes the distribution of Zn isotopes in Fanjia river system. While a large number of carbonate minerals provide conditions for Zn to be adsorbed or precipitated into sediment in the natural state, which leads to heavy Zn isotope preferentially enters the solid phase. Observations by Mavromatis et al. (2019) confirmed that heavy Zn isotopes are preferentially released into the solid phase when Zn was co-precipitated with carbonate.

Changes of Zn concentration and isotope composition in sediments and paddy soils reveal the degree of Zn pollution in the lateral dimension. Remarkably, the high Zn content that present in carbonate fraction implies the high re-release risk of Zn (Fig. 2). Generally, a mixture of Zn from different sources determines the observed variations in Zn concentration and Zn isotope ratio (e.g. Zhao et al., 2014; Araújo et al., 2019). In the plot of δ^{66}Zn value versus 1/Zn (the inverse of Zn concentration) (Fig. 4), data of paddy soil and sediment can be qualitatively explained by the mixing of at least three end-members of Zn: end-member A with a high Zn abundance but a low δ^{66}Zn value, end-member B with an intermediate Zn concentration and a relatively high δ^{66}Zn value, and end-member C with a low Zn concentration but a high δ^{66}Zn value. It is observed that the tailing has a Zn concentration of 100.59 g/kg and δ^{66}Zn value of −0.42 ± 0.02‰ (Fig. 4), we can conclude that end-member A is most likely to be tailing. Zinc may via long-term wind dispersion of fine-grained material from the tailing (Bi et al., 2017; Del Rio-Salas et al., 2019). In addition, our data fall between three local components of mining input, agricultural input, and background. Previous studies have indicated that substances in the atmosphere in southwestern China may predominantly derived from natural sources, including carbonate and silicate dust and anthropogenic pollution such as fertilizer (Han and Liu, 2006; Han et al., 2011). Zinc isotope signal of dust may be controlled by fertilizer and mining input, including refining processes and wind dispersion of fine-grained materials from the tailing. So, we can propose that end-member B is likely to be dust. Yet a straightforward interpretation of the δ^{66}Zn data of geogenic soil is complicated by the fact that additional sources of Zn, such as dust and long-term influence of fertilizer, may have masked the local background Zn isotope signatures (Cloquet et al., 2008). Geogenic soil may represent Zn isotope signals of parent material, dust, and fertilizer. It can therefore be concluded that end-member C is geogenic soil. Therefore, the three direct end-members of Zn in sediment and paddy soil are tailing, dust, and geogenic soil, respectively. Zn of dust and geogenic soil is

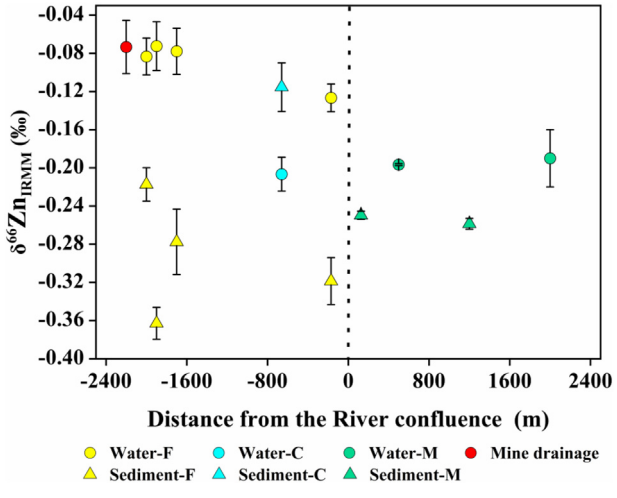

Fig. 3. δ^{66}Zn values vary with distance from the confluence of rivers in water and sediment ("F", "C", and "M" refer to Fanjia River, Caiyuan River, and mixing of both, respectively).

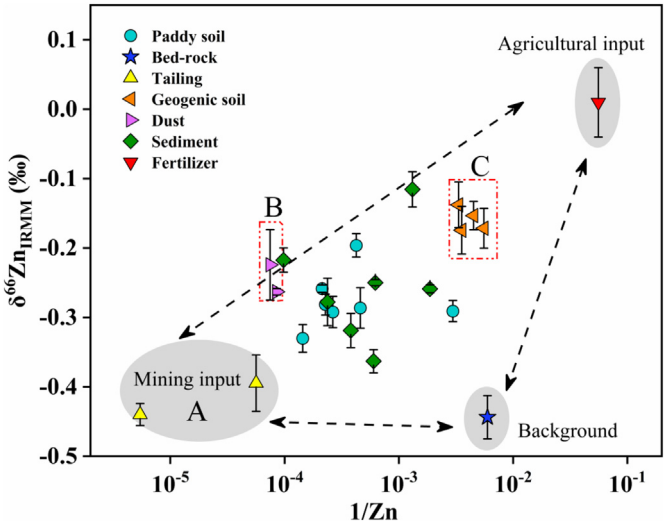

Fig. 4. δ^{66}Zn value as a function of 1/Zn molar ratios of samples.

the product of evolution. The proportions of Zn derived from these three end-members can be calculated through mixing equations.

$$Zn_{total} = x_A Zn_A + x_B Zn_B + Zn_C x_C$$

$$Zn_{total}\delta^{66}Zn = Zn_A\delta^{66}Zn_A x_A + Zn_B\delta^{66}Zn_B x_B + Zn_C\delta^{66}Zn_C x_C$$

$$1 = x_A + x_B + x_C$$

where A, B, and C represent the three end-members of tailing, dust, and geogenic soil, respectively; x_A, x_B, and x_C are the proportion of each end-member.

Based on the equations above, the contributions from three end-members to the paddy soils and sediments were calculated using a MATLAB program. The calculated results are present in Fig. 5. Results show that the contribution of geogenic soil in paddy soils is the main one, with an average value of 80%. Dust contributes most of the anthropogenic Zn with an average value of 18.6%. The total contribution of anthropogenic Zn shows a downward trend from site #1 to #8, with increasing distance from the mining area. Similarly, dust appears to be the main anthropogenic sources in sediments with a high proportion of 90.9% in site #2, then decreased with increasing distance from the mining area. In general, dust is the dominant source for anthropogenic Zn in our study area. This finding would help understanding that to remediate soil pollution by heavy metals in karst area, the large amount of dust generated in the mining area is the first problem need to be solved.

5.2. Zinc behaviors in paddy soil profile

Dissolved Zn migrate from the surface to deeper part of the soil profile, which may cause the pollution of deep soil (Kong et al., 2018) or even groundwater (Sherene, 2010). It is, therefore, important to understand how Zn migrates in the vertical soil profile. As for HP profile, the surface horizon is clearly impacted by the mining-derived deposition as could be indicated by the high Zn concentration and low δ^{66}Zn value. Zinc concentrations decrease with depth but the δ^{66}Zn values have limited change at the upper horizon soils (0–60 cm) (Fig. 6A). However, the δ^{66}Zn value of the deepest soil horizon deviates this trend and is identical to that of the geogenic soil. This indicates that soils at the depth of 0–60 cm are entirely affected by the mining-derived Zn deposited on the surface. By contrast, the anthropogenic influence on the soils from the deeper horizon (>60 cm) is limited. As for MP profile, at the depth of 0–40 cm horizon in MP profile, Zn concentration and δ^{66}Zn value of soil have insignificant change with depth (Fig. 6B). At the depth of 40–80 cm, Zn concentration decreases with depth, while the δ^{66}Zn value shows only minor shifts to heavier but still between that of upper layer soil (0–40 cm) and the geogenic soil. This indicates that the Zn of 40–80 cm horizon comes from the mixing of the Zn leached from the surface and native Zn. All those results show that the Zn of the topsoil can migrate to the depth of ~40 cm in MP profile. Unlike the HP and MP profiles, the δ^{66}Zn values in LP profile are nearly unchanged and approach to the geogenic soil (Fig. 6C). The variation of δ^{66}Zn value and Zn concentration confirms that the Zn of LP profile is mainly derived from the "natural" long-term weathering of the bed-rocks, and is not (or only little) affected by the mining.

Clearly, the enrichment of Zn in profile may be related to large input of Zn from mining activities, but the behaviors of Zn are also affected by the proprieties of the soils and environmental conditions (Shaheen and Rinklebe, 2014). As shown in Fig. 2C, the comparable data of Zn extracted in carbonate fraction of three profiles indicate that Zn shows low chemical mobility and bio-availability in the process of soil formation. However, the mining activities bring heavy metals buried underground to the surface. The subtropical climate and high permeability of karst aquifers accelerate the migration of heavy metals and enhance their activity (Kong et al., 2018). Zinc concentration of soil in MP and LP profile as well as at the depth of >60 cm in HP profile, is positively correlated with the abundance of Fe & Al, while significantly anti-correlated with Ca & Mg (Fig. 6). Similar positive relationships were reported between soil clay, total Al, total Fe and As, Cd, Cr, Mo, Se, V, and Zn (Shaheen and Rinklebe, 2014, 2018; Rinklebe et al., 2016; Shaheen

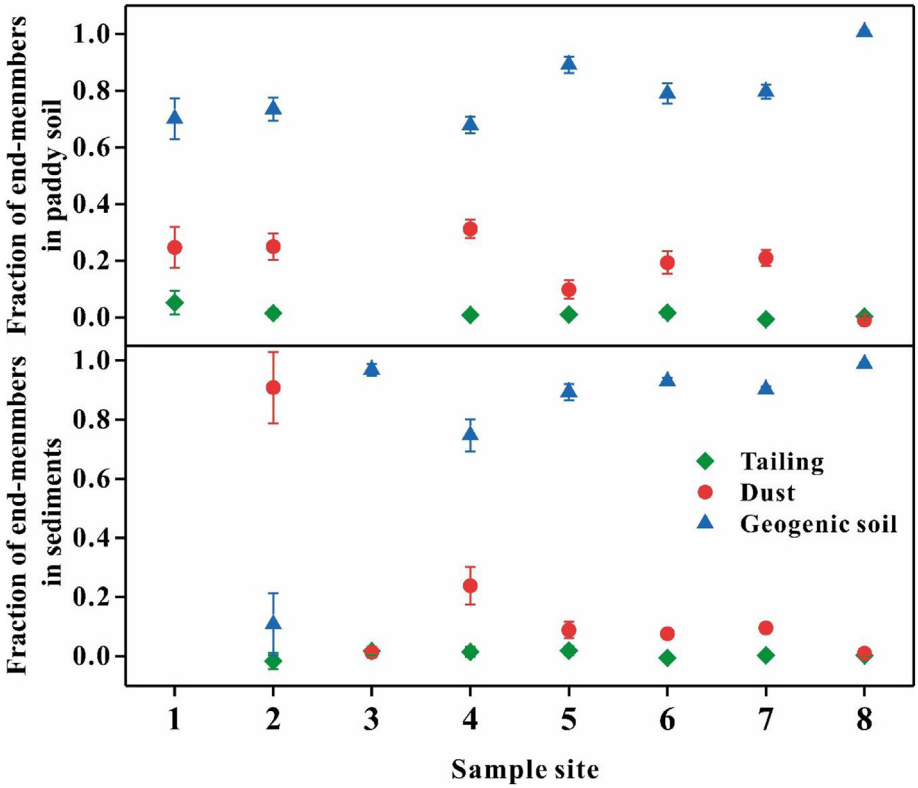

Fig. 5. The contributions from three end-members in paddy soil and sediment.

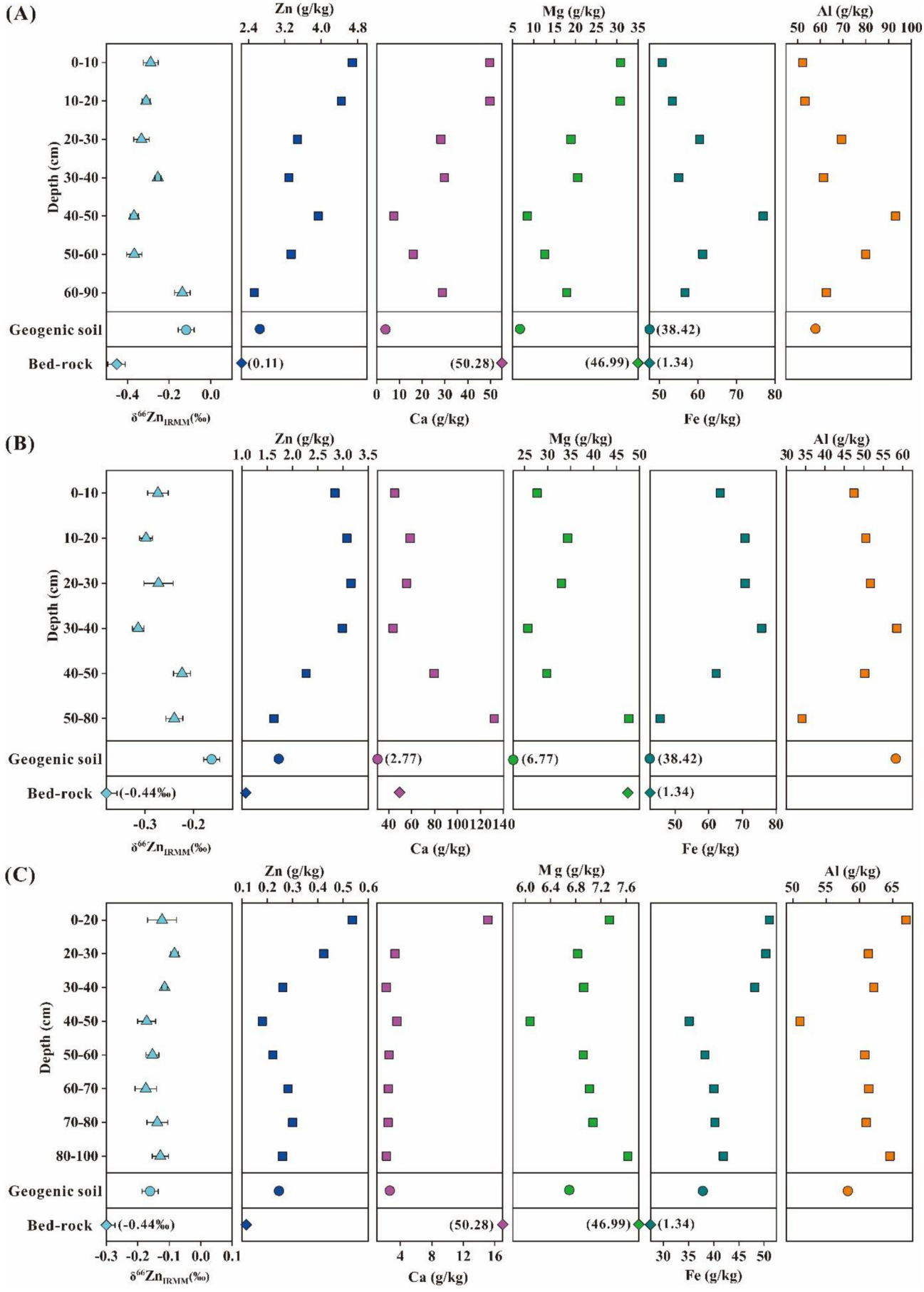

Fig. 6. Depth distribution of metal element concentrations and $\delta^{66}Zn$ values in the three soil profiles (A: HP profile; B: MP profile; C: LP profile).

et al., 2017). This strong impact of total Fe and Al on Zn indicates that Zn is associated (bounded and/or occluded) with Fe-Al oxides (Rinklebe et al., 2016, 2019), which shows the controlling effect of Fe-Al oxides on the migration of Zn in profile. Especially, upper soils (0–60 cm) of HP profile follow an opposite trend due to the significant effect of mining activities. In other words, Zn concentration is no longer dominantly controlled by Fe-Al oxides, but related to the forcible inputs due to the mining activities. We also found that the Fe-Al oxides associated with Zn only had minor effects on the δ^{66}Zn values. This is consistent the conclusion of Pokrovsky et al. (2005) who demonstrated that adsorption reactions only contribute to a minor degree to Zn isotope fractionation in natural settings. This confirms that it is available to trace Zn sources through surface soil in karst area as Zn isotope fractionate limitedly during the migration of Zn in soil profile. Similar findings were reported by Bigalke et al. (2010) who observed that the fractionation of Zn isotopes during transport of Zn through soil profile was weak.

Taken together, we conclude that the closer to the mining area, the more active the migration of Zn. Mining activities bring the underground heavy metals to the surface, which enhances their activity under the special hydrogeological conditions of karst. The absolute content of Zn input by mining is high and the amount of leaching Zn increases accordingly, which may result from the high permeability of karst landforms. The Fe-Al oxides impact on the migration of Zn in profile but do not lead to significant Zn isotopes fractionation.

6. Conclusions

The emission of heavy metals from mining and metallurgy activities has become an important environmental issue. Tracing anthropogenic sources and identifying the migration route of heavy metals are critical to develop strategies to reduce the accumulation of metals effectively. Our findings demonstrate that the mine drainage has a limited impact on river water. Instead, dust is the dominant source for anthropogenic Zn in our study area. Zinc from mining enters paddy soil and sediment via long-term wind dispersion of fine-grained material from the tailing, as well as the atmospheric deposition of dust. The effect of S transformation in Zn ore on heavy metal migration has been weakened in the karst area. Our findings also demonstrate that under the special hydrogeological conditions of karst, mining activities will increase the migration of heavy metals and thus increase their ecological risks. The Fe-Al oxides control the migration of Zn in soil profile but do not lead to significantly Zn isotope fractionation.

CRediT authorship contribution statement

Yafei Xia: Investigation, Data curation, Writing - original draft. **Ting Gao:** Conceptualization, Writing - review & editing. **Yuhui Liu:** Investigation, Methodology. **Zhengrong Wang:** Formal analysis. **Chengshuai Liu:** Supervision. **Qiqi Wu:** Project administration. **Meng Qi:** Project administration. **Yiwen Lv:** Funding acquisition. **Fangbai Li:** Resources.

Declaration of competing interest

The authors declare that they have no known competing financial interests or personal relationships that could have appeared to influence the work reported in this paper.

Acknowledgments

We thank Dr. Yang Tang for help in the MC-ICPMS lab. This work was financially supported by the National Natural Science Foundation of China (U1701241 and 41701266), the Key Scientific Research Projects of the Chinese Academy of Sciences (QYZDB-SSW-DQC046), the GDAS' Project of Science and Technology Development (2019GDASYL-0104016 and 2019GDASYL-0103048), the Science and Technology Planning Project of Guangdong Province, China (2017BT01Z176 and 2017B030314092), and the Construction Project of Modern Agricultural Science and Technology Innovation Alliance of Guangdong Province, China (2016LM2149).

References

Aranda, S., Borrok, D.M., Wanty, R.B., Balistrieri, L.S., 2012. Zinc isotope investigation of surface and pore waters in a mountain watershed impacted by acid rock drainage. Sci. Total Environ. 420, 202–213.
Araújo, D.F., Boaventura, G.R., Machado, W., et al., 2017. Tracing of anthropogenic zinc sources in coastal environments using stable isotope composition. Chem. Geol. 449, 226–235.
Araújo, D.F., Ponzevera, E., Briant, N., et al., 2019. Assessment of the metal contamination evolution in the Loire estuary using Cu and Zn stable isotopes and geochemical data in sediments. Mar. Pollut. Bull. 143, 12–23.
Arnold, T., Markovic, T., Kirk, G., et al., 2015. Iron and zinc isotope fractionation during uptake and translocation in rice (Oryza sativa) grown in oxic and anoxic soils. Compt. Rendus Geosci. 347, 397–404.
Aucour, A.M., Bedell, J.P., Queyron, M., et al., 2017. Zn speciation and stable isotope fractionation in a contaminated urban wetland soil–typha latifolia system. Environmental Science & Technology 51, 8350–8358.
Balistrieri, L.S., Borrok, D.M., Wanty, R.B., Ridley, W.I., 2008. Fractionation of Cu and Zn isotopes during adsorption onto amorphous Fe(III) oxyhydroxide: experimental mixing of acid rock drainage and ambient river water. Geochim. Cosmochim. Acta 72, 311–328.
Bi, X.Y., Li, Z.G., Wang, S.X., et al., 2017. Lead isotopic compositions of selected coals, Pb/Zn ores and fuels in China and the application for source tracing. Environmental Science & Technology 51, 13502–13508.
Bigalke, M., Weyer, S., Kobza, J., Wilcke, W., 2010. Stable Cu and Zn isotope ratios as tracers of sources and transport of Cu and Zn in contaminated soil. Geochim. Cosmochim. Acta 74, 6801–6813.
Bigalke, M., Kersten, M., Weyer, S., Wilcke, W., 2013. Isotopes trace biogeochemistry and sources of Cu and Zn in an intertidal soil. Soil Sci. Soc. Am. J. 77, 680.
Borrok, D.M., Wanty, R.B., Ridley, W.I., Wolf, R., Lamothe, P.J., Adams, M., 2007. Separation of copper, iron, and zinc from complex aqueous solutions for isotopic measurement. Chem. Geol. 242, 400–414.
Bridgestock, L.J., Williams, H., Rehkämper, et al., 2014. Unlocking the zinc isotope systematics of iron meteorites. Earth Planet. Sci. Lett. 400, 153–164.
Chen, H.Y., Teng, Y.G., Lu, S.J., et al., 2015. Contamination features and health risk of soil heavy metals in China. Sci. Total Environ. 512, 143.
Cloquet, C., Carignan, J., Lehmann, M.F., Vanhaecke, F., 2008. Variation in the isotopic composition of zinc in the natural environment and the use of zinc isotopes in biogeosciences: a review. Anal. Bioanal. Chem. 390, 451–463.
Del Rio-Salas, R., Ayala-Ramírez, Y., Loredo-Portales, R., et al., 2019. Mineralogy and geochemistry of rural road dust and nearby mine tailings: a case of ignored pollution hazard from an abandoned mining site in semi-arid zone. Nat. Resour. Res. 28, 1485–1503.
Dorin, Bunce, N.J., 2015. Acid mine drainage: electrochemical approaches to prevention and remediation of acidity and toxic metals. J. Appl. Electrochem. 45, 1239–1254.
Fekiacova, Z., Cornu, S., Pichat, S., 2015. Tracing contamination sources in soils with Cu and Zn isotopic ratios. Sci. Total Environ. 517, 96–105.
Fernandez, A., Borrok, D.M., 2009. Fractionation of Cu, Fe, and Zn isotopes during the oxidative weathering of sulfide-rich rocks. Chem. Geol. 264, 1–12.
Flora, A., Emma, F.C., Cerqueira, B., Andrade, M.L., 2011. Migration rates of Cd, Cu and Pb in different soil profiles. Fresenius Environ. Bull. 20.
Franssens, M., Flament, P., Deboudt, K., Weis, D., Perdrix, E., 2004. Evidencing lead deposition at the urban scale using "short-lived" isotopic signatures of the source term (Pb-Zn refinery). Atmos. Environ. 38, 5157–5168.
Gao, T., Ke, S., Wang, S.J., et al., 2018. Contrasting Mg isotopic compositions between Fe-Mn nodules and surrounding soils: accumulation of light Mg isotopes by Mg-depleted clay minerals and Fe oxides. Geochim. Cosmochim. Acta 237, 205–222.
Guagliardi, I., Cicchella, D., De Rosa, R., et al., 2015. Assessment of lead pollution in topsoils of a southern Italy area: analysis of urban and peri-urban environment. J. Environ. Sci. (China) 33, 179–187.
Han, G., Liu, C.Q., 2006. Strontium isotope and major ion chemistry of the rainwaters from Guiyang, Guizhou Province, China. Sci. Total Environ. 364, 165–174.
Han, G., Wu, Q., Tang, Y., 2011. Acid rain and alkalization in southwester China: chemical and strontium isotope evidence in rainwater from Guiyang. J. Atmos. Chem. 68, 139–155.
Juillot, F., Maréchal, C., Morin, G., et al., 2011. Contrasting isotopic signatures between anthropogenic and geogenic Zn and evidence for post-depositional fractionation processes in smelter-impacted soils from Northern France. Geochim. Cosmochim. Acta 75, 2295–2308.
Khalil, A., Hanich, L., Hakkou, R., et al., 2014. GIS-based environmental database for assessing the mine pollution: a case study of an abandoned mine site in Morocco. J. Geochem. Explor. 144, 468–477.
Kong, J., Guo, Q., Wei, R., et al., 2018. Contamination of heavy metals and isotopic tracing of Pb in surface and profile soils in a polluted farmland from a typical karst area in southern China. Sci. Total Environ. 637–638, 1035–1045.
Lewis, W., 2004. Dissolution: Carbonate rocks. Encyclopedia of Caves and Karst Science. 7, pp. 608–621.
Li, Z., Ma, Z., Kuijp, T.J., Yuan, Z., Huang, L., 2014. A review of soil heavy metal pollution from mines in China: pollution and health risk assessment. Sci. Total Environ. 468–469, 843–853.

Li, X., Yang, H., Zhang, C., et al., 2017. Spatial distribution and transport characteristics of heavy metals around an antimony mine area in central China. Chemosphere 170, 17–24.
Li, W., Gou, W., Li, W., et al., 2019. Environmental applications of metal stable isotopes: silver, mercury and zinc. Environnental Pollution 252, 1344–1356.
Liu, S.A., Wang, Z.Z., Li, S.G., Huang, J., Yang, W., 2016. Zinc isotope evidence for a large-scale carbonated mantle beneath eastern China. Earth Planet. Sci. Lett. 444, 169–178.
Lv, Y., Liu, S.A., Zhu, J.M., Li, S., 2016. Copper and zinc isotope fractionation during deposition and weathering of highly metalliferous black shales in central China. Chem. Geol. 445, 24–35.
Marechal, C.N., Telouk, P., Albarede, F., 1999. Precise analysis of copper and zinc isotopic compositions by plasma-source mass spectrometry. Chem. Geol. 156, 251–273.
Marrugo-Negrete, J., Pinedo-Hernández, J., Díez, S., 2017. Assessment of heavy metal pollution, spatial distribution and origin in agricultural soils along the Sinú River Basin, Colombia. Environ. Res. 154, 380–388.
Mavromatis, V., González, A.G., Dietzel, M., Schott, J., 2019. Zinc isotope fractionation during the inorganic precipitation of calcite-towards a new pH proxy. Geochim. Cosmochim. Acta 244, 99–112.
Moore, O.W., Buss, H.L., Green, S.M., Liu, M., Song, Z., 2017. The importance of non-carbonate mineral weathering as a soil formation mechanism within a karst weathering profile in the SPECTRA Critical Zone Observatory, Guizhou Province, China. Acta Geochimica 36, 566–571.
Moynier, F., Vance, D., Fujii, T., Savage, P., 2017. The isotope geochemistry of zinc and copper. Rev. Mineral. Geochem. 82, 543–600.
Peng, T., Wang, Sj, 2012. Effects of land use, land cover and rainfall regimes on the surface runoff and soil loss on karst slopes in southwest China. Catena 90, 53–62.
Pokrovsky, O.S., Viers, J., Freydier, R., 2005. Zinc stable isotope fractionation during its adsorption on oxides and hydroxides. J. Colloid Interface Sci. 291, 192–200.
Pons, M.L., Quitte, G., Fujii, T., et al., 2011. Early Archean serpentine mud volcanoes at Isua, Greenland, as a niche for early life. Proc. Natl. Acad. Sci. U. S. A. 108, 17639–17643.
Pons, M.L., Fujii, T., Rosing, M., Quitte, G., Telouk, P., Albarede, F., 2013. A Zn isotope perspective on the rise of continents. Geobiology 11, 201–214.
Pu, Y.L., Tu, Y.R., You, Z.H., et al., 2017. Application of Pb-Zn isotope in the analysis of heavy metal pollution sources in sediments: review and prospect. Environ. Chem. 36 (3), 581–590.
Pu, W., Sun, J., Zhang, F., Wen, X., Liu, W., Huang, C., 2019. Effects of copper mining on heavy metal contamination in a rice agrosystem in the Xiaojiang River Basin, southwest China. Acta Geochimica 38, 753–773.
Qin, Z.J., Lin, Y.S., Yuan, D.X., et al., 2012. A discussion on mine and water pollution problems in karst areas in southwest China. Acta Geosci. Sin. 33 (3), 341–348.
Rinklebe, J., Shaheen, S.M., Schroter, F., Rennert, T., 2016. Exploiting biogeochemical and spectroscopic techniques to assess the geochemical distribution and release dynamics of chromium and lead in a contaminated floodplain soil. Chemosphere 150, 390–397.
Rinklebe, J., Antoniadis, V., Shaheen, S.M., Rosche, O., Altermann, M., 2019. Health risk assessment of potentially toxic elements in soils along the Central Elbe River, Germany. Environ. Int. 126, 76–88.
Ruan, Y.L., Lian, B., An, Y.L., et al., 2013. Ecological environment protection and sustainable development in karst area. Earth and Environment 41 (4), 388–396.
Shaheen, S.M., Rinklebe, J., 2014. Geochemical fractions of chromium, copper, and zinc and their vertical distribution in floodplain soil profiles along the Central Elbe River, Germany. Geoderma 228–229, 142–159.
Shaheen, S.M., Rinklebe, J., 2018. Vanadium in thirteen different soil profiles originating from Germany and Egypt: geochemical fractionation and potential mobilization. Appl. Geochem. 88, 288–301.
Shaheen, S.M., Kwon, E.E., Biswas, J.K., et al., 2017. Arsenic, chromium, molybdenum, and selenium: geochemical fractions and potential mobilization in riverine soil profiles originating from Germany and Egypt. Chemosphere 180, 553–563.
Sherene, T., 2010. Mobility and transport of heavy metals in polluted soil environment. Biological Forum 2, 112–121.
Sieber, M., Conway, T.M., de Souza, G.F., Hassler, C.S., Ellwood, M.J., Vance, D., 2020. Cycling of zinc and its isotopes across multiple zones of the Southern Ocean: insights from the Antarctic Circumnavigation Expedition. Geochim. Cosmochim. Acta 268, 310–324.
Simate, G.S., Ndlovu, S., 2014. Acid mine drainage: challenges and opportunities. Journal of Environmental Chemical Engineering 2, 1785–1803.
Stromberg, Banwart, 1999. Weathering kinetics of waste rock from the Aitik copper mine, Sweden: scale dependent rate factors and pH controls in large column experiments. J. Contam. Hydrol. 39, 59–89.
Sun, J., Yu, R., Hu, G., Su, G., Zhang, Y., 2018. Tracing of heavy metal sources and mobility in a soil depth profile via isotopic variation of Pb and Sr. Catena 171, 440–449.
Tessier, Campbell, Bisson, M., 1979. Sequential extraction procedure for the speciation of particulate trace metals. Anal. Chem. 51.
Vance, D., de Souza, G.F., Zhao, Y., Cullen, J.T., Lohan, M.C., 2019. The relationship between zinc, its isotopes, and the major nutrients in the North-East Pacific. Earth Planet. Sci. Lett. 525.
Viers, J., Prokushkin, A.S., Pokrovsky, O.S., et al., 2015. Zn isotope fractionation in a pristine larch forest on permafrost-dominated soils in Central Siberia. Geochem. Trans. 16, 3.
Wang, S.J., Liu, Q.M., Zhang, D.F., 2004. Karst rocky desertification in southwestern China: geomorphology, landuse, impact and rehabilitation. Land Degrad. Dev. 15, 115–121.
Wang, Z.Z., Liu, S.A., Liu, J., et al., 2017. Zinc isotope fractionation during mantle melting and constraints on the Zn isotope composition of Earth's upper mantle. Geochim. Cosmochim. Acta 198, 151–167.
Wiederhold, J.G., 2015. Metal stable isotope signatures as tracers in environmental geochemistry. Environmental Science & Technology 49, 2606–2624.
Wiggenhauser, M., Bigalke, M., Imseng, M., et al., 2018. Zinc isotope fractionation during grain filling of wheat and a comparison of zinc and cadmium isotope ratios in identical soil-plant systems. New Phytol. 219, 195–205.
Yang, W.J., Ding, K.B., Zhang, P., et al., 2019. Cadmium stable isotope variation in a mountain area impacted by acid mine drainage. Sci. Total Environ. 646, 696–703.
Ye, L., 2001. Discussion on the distribution and occurrence of cadmium in the cadmium and zinc rich deposit in niujiaotang, Duyun, Guizhou. Acta Mineralogica Sinca 21.
Yun, S.W., Baveye, P.C., Kim, K.B., et al., 2016. Effect of postmining land use on the spatial distribution of metal(loid)s and their transport in agricultural soils: analysis of a case study of Chungyang, South Korea. J. Geochem. Explor. 170, 157–166.
Zhang, L., Qin, X., Tan, J., et al., 2016. Review ofarsenic geochemical characteristics and its significance on arsenic pollution studies in karst groundwater, Southwest China. Appl. Geochem. 77, 80–88.
Zhang, J., Wei, H.R., Yang, R.D., Gao, J.B., Ou, Y.H., 2018. Distribution characteristics of heavy metal elements in beneficiation tailings of Niujiaotang lead-zinc mine in Duyun. Guizhou. Nonferrous Metal Engineering 8 (1), 122–127.
Zhao, Y., Vance, D., Abouchami, W., de Baar, H.J.W., 2014. Biogeochemical cycling of zinc and its isotopes in the Southern Ocean. Geochim. Cosmochim. Acta 125, 653–672.